Title

Attosecond time delays in the body frame for photodetachment from molecular anions

Journal

Physical Review A, 110(1)

ISSN

2469-9926

Authors

Rescigno, Thomas N

Trevisan, Cynthia S

Lucchese, Robert R

et al.

Publication Date

2024-07-01

DOI

10.1103/physreva.110.013122

Attosecond time delays in the body frame for photodetachment from molecular anions

Thomas N. Rescigno,[1] Cynthia S. Trevisan,[2,1] Robert R. Lucchese,[1] and C. William McCurdy[3,1]
[1]*Chemical Sciences Division, Lawrence Berkeley National Laboratory, Berkeley, California 94720, USA*
[2]*Department of Sciences and Mathematics, California State University Maritime Academy, Vallejo, California 94590, USA*
[3]*Department of Chemistry, University of California, Davis, California 95616, USA*

Attosecond time delays in molecular photoionization at low energies are dominated by the contribution of the Coulomb phase, which diverges as the energy of the photoelectron decreases towards zero. With calculations on core-electron ejection from CN^- and C_2^- we demonstrate that in photodetachment of molecular anions the absence of the long-range Coulomb interaction in the final state can reveal the delays of narrow low-energy shape resonances that do not generally occur in photoionization. Delays of several femtoseconds can be associated with such resonances. The angular dependence of photodetachment time delays in the body frame is highly sensitive to short-range anisotropies in the electron-molecule interaction as well as to the initial state.

I. INTRODUCTION

Since the electron-ion scattering continuum is the final state for photoionization, the dynamics of that process is dominated by the Coulomb interaction between the outgoing electron and the residual ion. As a result, the theoretical description of photoionization is partially simplified by the dominant long-range Coulomb potential which diminishes the relative importance of electron correlation and long-range polarization, especially at low energy. In contrast, for photodetachment of electrons from molecular anions, where the relevant scattering continuum is that of electron-neutral molecule scattering, correlation and long-range polarization effects dominate the dynamics at low energy.

The measurement of photoelectron distributions in the molecular frame [1] and, more recently, the measurement of attosecond time delays [2–7] have allowed richly detailed interpretations of molecular photoionization. In particular, observation of photoionization time delays on the attosecond scale has opened the way for experimental access to the energy dependence of the phases of quantum-mechanical amplitudes for photoemission. However, below a few electron volts, where the intrinsically molecular aspects of the process can be strongest, that new view of photoionization dynamics is partly obscured by the dominant contribution to the phase of the amplitude that is due to the Coulomb interaction of the outgoing electron and the residual ion.

Extending time delay measurements, including their angular dependence in the molecular frame, to photodetachment of molecular anions can provide a more powerful view of low-energy electron-molecule interactions than has previously been available. Attosecond time delay observations in photodetachment will probe low-energy shape resonances with longer lifetimes than are typical in photoionization, as well as excitation threshold dynamics, and long-range interactions. Such measurements will provide a powerful test of theoretical treatments of photodetachment. In this paper we explore time delays in core-electron photodetachment of CN^- and C_2^- anions as examples of the physics that time delay observations can reveal, and also attempt to address some of the challenges to theoretical predictions of time delays posed by photodetachment.

Much of the experimental and theoretical foundation for the study of photodetachment time delays has been laid in the recent literature on photoionization time delays. Starting from the measurement and interpretation of delay differences of a few tens of attoseconds in photoionization from different electronic energy levels in atoms [5,6], experiment and theory rapidly evolved to interpret the appearance of photoionization resonances in time delay measurements [8–12]. The fundamental physics of time delays and their measurement has become the subject of extensive investigation [7,13–20]. The angular dependence of photoionization time delays has also been explored in several contexts [10,11,21], including through measurements and theoretical predictions of the angular dependence of delays in the body frame of a molecule [12]. The understanding of the information accessible through time delays has been further enhanced by measurement and theory of the photoionization of dimers [22] and larger clusters [23].

There has been much less work on the subject of time delays in photodetachment of anions, most of it on atoms, and that work provides impetus for our present paper. Lindroth and Dahlström [24] calculated time delays for photodetachment of the F^- and Cl^- anions, and analyzed the fundamental differences between measurement of photodetachment delays in experiments using reconstruction of attosecond beating by interference of two-photon transitions (RABBITT) [25] and the analogous measurements for photoionization delays. Saha *et al.* [26,27] have given relativistic theoretical treatments of photodetachment delays in atomic Cl^-.

In all studies of attosecond time delays in photoionization or photodetachment the target of measurements is the delay due to the energy dependence of the phase of the photoabsorption matrix element [2,7]:

$$\tau(\hat{k},\hat{\epsilon}) = \hbar\frac{\partial}{\partial E_k}\arg\left\langle \Psi^-_{\Gamma_0,\mathbf{k}}\middle|\hat{\epsilon}\cdot\boldsymbol{\mu}|\Psi_0\right\rangle \qquad (1)$$

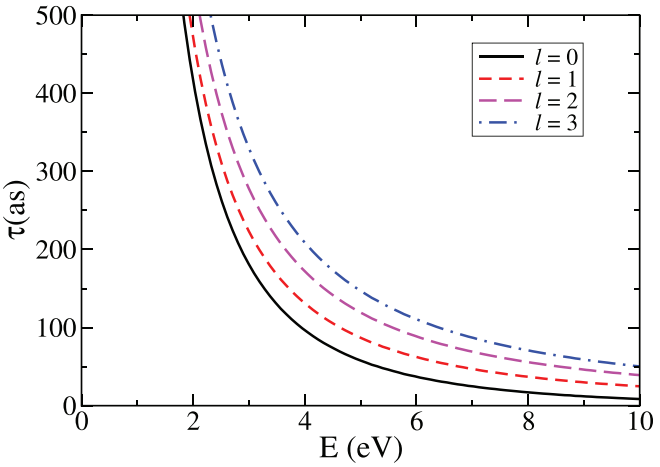

FIG. 1. Attosecond delays due to a pure Coulomb phase of different angular momenta as a function of electron kinetic energy for an attractive Coulomb potential with unit charge.

where $\boldsymbol{\mu}$ is the dipole operator, $\hat{\epsilon}$ is the polarization, Ψ_0 is the initial state of the target, and $\Psi^-_{\Gamma_0,\mathbf{k}}$ is the electron-ion (or, in the case of photodetachment, electron-neutral) scattering wave function with incoming boundary conditions labeled by the momentum, $\mathbf{k}$, of the electron and the ionization channel, Γ_0. In both atomic and molecular photoionization there is a contribution to the phase of the dipole matrix element from the Coulomb scattering phase shift for all the angular momenta, ℓ, involved in the matrix element:

$$\sigma_\ell(k) = \arg\Gamma(\ell + 1 + i\eta). \tag{2}$$

Here k is the momentum of the electron and $\eta = -\frac{Ze^2m}{\hbar^2 k}$, where Ze is the charge of the residual positive ion and m is the electron mass. As the photoelectron kinetic energy decreases below 5 eV, the pure Coulomb delay, shown in Fig. 1, rises continuously from about 50 as to hundreds of attoseconds at 1 or 2 eV before going to infinity at $E = 0$. Even though measurements of photoionization time delays are generally relative, the large Coulomb contribution can obscure low-energy features. However, the difference between time delays for photodetachment and photoionization is still more fundamental. As we will demonstrate in the two examples we study here, low-energy features like long-lived shape resonances can abound in photodetachment, as well as strong anisotropies in the angular dependence of the time delay that are sensitive to both short- and long-range details of the final-state interaction, while these are far less common in photoionization.

Since we are investigating the physical origins of the body-frame angular dependence of the photodetachment time delay, we focus on detachment of a core electron from molecular anions. The resulting neutral molecule that is produced has a core vacancy that can Auger decay to dissociate the molecule and produce at least one charged fragment. Coincidence measurements using momentum imaging [28–30] are thus a way in which the body-frame time delays could be accessed. In addition, photoemission from core levels is a localized probe of the emission dynamics, providing a possibly easier path to physical interpretation of the process.

Since the definition of photoemission time delay is somewhat different from the more familiar Eisenbud-Wigner-Smith time delay [31–33] in scattering theory, in the following section we will briefly summarize the connection of the photodetachment time delay and the multichannel electron-molecule scattering wave function, and also review the complex Kohn variational method we use to calculate those time delays including the effects of electron correlation. In Sec. III we discuss the results of our calculations on core photodetachment of the C_2^- anion, and the role of channel coupling in that example. Section IV reports our results for time delays in detachment from either the C or N core in the cyanide anion. We conclude with a discussion of the interpretation of photodetachment time delays in Sec. V.

II. THEORY AND COMPUTATION

A. Body-frame photoemission delays

Time delays in attosecond photoejection of electrons from molecules generally depend on the direction in the molecular frame of the final momentum of the electron. It will be useful here to review specifically how that angular dependence arises and how it emerges from the combination of the multichannel electron-molecule scattering wave function that we calculate using the complex Kohn variational method and the wave function of the bound initial electronic state.

After the original references [31–33] an extensive literature on Eisbud-Wigner-Smith time delays appeared, first addressing questions of their physical meanings, and later stimulated by the questions posed by the development of methods for measuring them in the photoejection of electrons. At a fundamental level a detailed review of the theoretical underpinnings of time delays by de Carvalho and Nussenzveig [34] reconciles the ideas of scattering time delays with the notion of "dwell time" and explains how the derivative of the phase of the scattering amplitude in a particular direction defines the time delay for scattering in that direction relative to an unscattered wave packet (a result also derived in 1972 by Nussenzveig [35]).

A more recent review of delays in photoejection by Pazourek, Nagele, and Burgdörfer [2] provides one derivation of Eq. (1) and discusses the physical manifestation of photoejection delays in streaking experiments both for short-range and Coulomb potentials. Since there is no physically realizable reference wave packet in the case of photoejection of electrons, the physically measurable meaning of the time delays is demonstrated in that review by considering the evolution in time of the expectation value of distance for the outgoing packet produced by a 200-as radiation pulse in two model systems. The result is a demonstration that IR streaking measurements can measure the delay defined by Eq. (1) for the cases of both short-range and Coulomb potentials despite the formal difficulties posed by the long-range nature of the Coulomb interaction.

Still more recently, a number of studies explore aspects of two-photon experimental determinations of photoionization time delays [7–10,17,20,21]. The question of how such measurements can be used to explore photoionization delays in the molecular frame has also been explored [12,15].

Here, our calculations of photodetachment time delays are based on multichannel electron-molecule scattering wave functions. We need only take the first steps in the treatments like those in Refs. [2,7], for example, to see how the outgoing wave packet of a photoelectron after a short radiation pulse appears as a superposition of time-independent N-electron scattering eigenfunctions, $\psi^-_{\Gamma,\vec{k}_\Gamma}(\mathbf{r}_1 \cdots \mathbf{r}_N)$, of energy E_k with incoming wave boundary conditions. If the scattering eigenfunctions are labeled by the momentum $\vec{k}_\Gamma$ in the channel labeled by electronic state Γ, the outgoing wave packet has the general form

$$\Psi(\mathbf{r}_1 \cdots \mathbf{r}_N, t) = \sum_\Gamma{}' \int d^3k\, C_\Gamma(\vec{k}_\Gamma, t)\, \psi^-_{\Gamma,\vec{k}_\Gamma}(\mathbf{r}_1 \cdots \mathbf{r}_N)\, e^{-iE_{k_\Gamma} t/\hbar}. \quad (3)$$

We take the scattering wave functions to be momentum normalized, and the primed sum goes over energetically open photoejection channels. For single-photon absorption, the coefficients $C_\Gamma(\vec{k}_\Gamma, t)$ are given by first-order time-dependent perturbation theory for the perturbation due to the pulse, $e\sum_i^N \boldsymbol{\epsilon}\cdot\mathbf{r}_i\,\mathscr{E}(t)$, in the length gauge as

$$C_\Gamma(\vec{k}_\Gamma, t) = -\frac{i}{\hbar}\langle\psi^-_{\Gamma,\vec{k}_\Gamma}|e\sum_i^N \hat{\epsilon}\cdot\mathbf{r}_i|\Phi_0\rangle \times \int_{-\infty}^{t} e^{(E_{k_\Gamma}-E_0)t'/\hbar}\mathscr{E}(t')dt'. \quad (4)$$

In Eq. (4) Φ_0 and E_0 are the initial electronic wave function and energy of the target molecule, E_{k_Γ} is the total energy of the scattering state, $\mathscr{E}(t)$ is the electric field of the attosecond pulse, $\hat{\epsilon}$ is its polarization, and e is the charge of the electron.

If the pulse is over by time $t = T$, then for times $t > T$ the packet in Eqs. (3) and (4) can be written as

$$\Psi(\mathbf{r}_1 \cdots \mathbf{r}_N, t) = \sum_\Gamma{}' \int d^3k\, D_\Gamma(\vec{k}_\Gamma)\, F(E_{k_\Gamma})\psi^-_{\Gamma,\vec{k}_\Gamma}(\mathbf{r}_1 \cdots \mathbf{r}_N)\, e^{-iE_k t/\hbar}, \quad (5)$$

where the dipole matrix element is denoted by $D_\Gamma(\vec{k}_\Gamma) = \langle\psi^-_{\Gamma,\vec{k}_\Gamma}|e\sum_i^N \hat{\epsilon}\cdot\mathbf{r}_i|\Phi_0\rangle$, and the envelope of the pulse in energy is

$$F\left(E_{k_\Gamma}\right) = -e\frac{i}{\hbar}\int_{-\infty}^{T} e^{(E_{k_\Gamma}-E_0)t/\hbar}\mathscr{E}(t)\,dt, \quad (6)$$

which we assume to be strongly peaked at $E_{k_\Gamma} = E_\Gamma + \hbar^2k_\Gamma^2/2m = \hbar\omega + E_0$, where m is the mass of the electron and ω is the central frequency of the laser pulse.

The product $D_\Gamma(\vec{k}_\Gamma)\,F(E_{k_\Gamma})$ in Eq. (5) is the key quantity that appears in the single-channel treatments of photoionization time delays in derivations [2,7] of Eq. (1). For appropriate choices of the parameters of an attosecond ionizing pulse, it is the energy dependence of the phase of the amplitude $D_\Gamma(\vec{k}_\Gamma)$ that determines the time delay [36] for electrons ejected in a given channel, and that amplitude can depend strongly on the direction of the outgoing momentum of the ejected electron in the body frame of the molecule.

The phase of the amplitude and its energy dependence is determined by both the final continuum state and the initial bound state and not by the scattering interaction alone. We will explore the consequences of that basic difference between photoejection and electron scattering delays further in Sec. V. The physics determining that directional dependence is potentially a sensitive probe of all aspects of the photoejection process, and if it can be measured it is the strongest currently available test of the theoretical description of photodetachment, because such experiments would yield direct information about both the magnitude and phase of the photoejection amplitude and their energy dependence.

Measuring the dependence on direction in the body frame for photoionization would seem to require orientation of the molecule by a method such as laser alignment [37–39], although at least one alternative to that approach that does not require prior alignment of the molecule has been demonstrated [12]. The case of photodetachment of molecular anions that we consider here, and for which we find particularly interesting molecular-frame angular dependence, poses additional challenges for prior alignment. For that reason we have focused on the detachment of core electrons. That process can be expected to be followed in many molecules by Auger decay of the neutral molecule within femtoseconds and subsequent dissociation into one positively charged and (at least) one neutral fragment. Recent progress suggests that experimental capabilities at x-ray free-electron laser facilities have reached the stage at which the observation of delays in the photodetachment of core electrons is becoming practical. For example, measurements of attosecond delays for photoemission from the oxygen K edge in x-ray core ionization of nitric oxide have been recently reported [40].

If the dissociation following Auger decay is prompt (more specifically, if it satisfies the "axial recoil" approximation [41,42]) then following the arguments in Ref. [2], for example, it should be possible in principle to perform a streaking observation of the ejected electron in coincidence with the detection of the positively charged fragment. Challenging as such an experiment or an equivalent one might be, we argue here that it would be strongly motivated by the potential to observe body-frame time delays that probe the electron-neutral molecule scattering continuum in unprecedented detail. However, as we find in the calculations described below, even measurements of photodetachment averaged over molecular anion orientations have the potential of observing delays of 1 fs or longer and thus probe the electron-molecule continuum in a striking time-dependent fashion.

Although the details of such measurements are beyond the scope of this paper, it is relevant to note here that the measurement of photodetachment delays from anions using the RABBITT technique [25] has been modeled and analyzed in depth already [24]. The measurement of photoemission delays using RABBITT depends on the absorption of two photons, generally one XUV photon from a high harmonic of the frequency of an IR photon, which in turn can be emitted or absorbed in the measurement. It has been shown that the measured atomic or molecular delay in photoemission, τ, can be separated into two contributions [43,44]:

$$\tau = \tau_W + \tau_{CC} \quad (7)$$

where τ_W is the "Wigner-like" delay due to the absorption of the XUV photon, and τ_{CC} is the continuum-continuum or Coulomb-laser coupling delay associated with the IR transition.

Lindroth and Dahlström [24] point out that the usual expression [44] for the continuum-continuum delay is zero in the absence of a Coulomb potential. Thus it is the short-range interactions of the emitted electron with the residual molecule or atom that determine τ_{CC}, and those are negligible at higher energies allowing direct measurement of τ_W which is the subject of our paper. On the other hand, below about 5 eV the short-range interactions with the residual neutral molecule may not be at all negligible, although given the estimates in Ref. [24] they would probably not obscure the large resonant delays we predict in Secs. III and IV. Thus, based on the existing analyses of the measurement of photodetachment delays, the molecular photodetachment delays we explore here are coming within the scope of practical measurements. At low energies, however, they will benefit from the support of theoretical predictions of the continuum-continuum delays if they are made using RABBITT.

We note that additional contributions to a measured time delay also occur in angular streaking experiments which have both continuum-continuum delays and contributions due to postcollision interactions which occur when the wave function of the emitted photoelectron is modified by the Auger decay event [40].

B. Complex Kohn variational calculations of photodetachment amplitudes

We calculate the required continuum wave functions in Eq. (1) using the well-established complex Kohn variational method for electron-molecule scattering [45] which can include coupling between the electronic states of the neutral molecule that define the photodetachment channels. These calculations are similar to photoionization calculations with the Kohn variational method which has been described previously [46–49], so we only describe the essential aspects of the method here.

In the case of C_2^- there are two nearly degenerate core orbitals and spin coupling to the unpaired valence electron creates four channels. Because CN^- is closed shell and the two core levels have very different energies, those two channels of core photodetachment can be treated in separate single-channel calculations. In general the electron-molecule scattering wave function is approximated by a close-coupling expansion:

$$\Psi^-_{\Gamma_o l_o m_o} = \sum_\Gamma \hat{A}\left(\chi_\Gamma F^-_{\Gamma\Gamma_o l_o m_o}\right) + \sum_i d_i^{\Gamma_0}\Theta_i, \tag{8}$$

where $\hat{A}$ is the antisymmetrization operator, the first sum over Γ runs over the N-electron electronic states of the neutral molecule being included, denoted by χ_Γ, and $F^-_{\Gamma\Gamma_o l_o m_o}$ is the corresponding photoelectron continuum function, with angular momentum quantum numbers l_o and m_o, for producing ion component Γ_o. The second sum runs over $(N+1)$-electron "penetration terms" built solely from target molecular orbitals and included in order to relax strong orthogonality constraints between target and continuum functions [45]. In the calculations described below, penetration terms were not required, so only the first sum in Eq. (8) was needed.

The one-electron continuum functions in the complex Kohn method are further expanded as

$$F^-_{\Gamma\Gamma_o l_o m_o} = \sum_i c_i^{\Gamma\Gamma_o}\phi_i(r) + \sum_{lm}\Big[f_l(k_\Gamma r)\delta_{ll_o}\delta_{mm_o}\delta_{\Gamma\Gamma_o} + T^{\Gamma\Gamma_o}_{ll_o mm_o} h_l^-(k_\Gamma r)\Big]Y_{lm}(\hat{r})/r\,, \tag{9}$$

where f_l and h_l^- are partial-wave continuum radial functions behaving asymptotically as regular and incoming spherical Bessel functions and ϕ_i is a set of square-integrable (Cartesian Gaussian) functions. An amplitude that represents a photodetachment process for a specific value of ejected electron momentum measured in the molecular body frame is constructed by combining the functions $\Psi^-_{\Gamma_o l_o m_o}$ in a partial-wave expansion:

$$\Psi^-_{\Gamma_0,\vec{k}_{\Gamma_0}} = \sum_{l_0 m_0} i^{l_0} Y^*_{l_0 m_0}(\hat{\mathbf{k}})\Psi^-_{k,\Gamma_0 l_0 m_0}(\mathbf{r}_1,\ldots,\mathbf{r}_N)\,. \tag{10}$$

The initial-state wave function of the anion target, Ψ_0, is constructed as a one determinant or correlated wave function constructed from the same orbitals as those used to represent the states of the neutral molecule.

The time delay, as defined in Eq. (1), is calculated by numerically differentiating the resulting amplitude $\langle\Psi^-_{\Gamma_0,\vec{k}_{\Gamma_0}}|\hat{\epsilon}\cdot\hat{\mu}|\Psi_0\rangle$ with respect to the photoelectron kinetic energy for a fixed direction of the polarization vector $\hat{\epsilon}$. The molecular frame photoelectron angular distribution (MFPAD) is related to the same dipole matrix element via the relation (in atomic units)

$$\frac{d^2\sigma^{\Gamma_0}}{d\Omega_{\hat{k}}d\Omega_{\hat{\epsilon}}} = \frac{8\pi\omega}{3c}\left|\left\langle\Psi^-_{\Gamma_0,\vec{k}_{\Gamma_0}}\middle|\hat{\epsilon}\cdot\hat{\mu}|\Psi_0\right\rangle\right|^2, \tag{11}$$

which defines the body-frame cross section for polarization $\hat{\epsilon}$ and ejected electron momentum $\vec{k}_{\Gamma_0}$, leaving the ion in state Γ_0. Then the orientation-averaged time delay is given by [15]

$$\tau = \frac{\int d\Omega_{\hat{k}}\int d\Omega_{\hat{\epsilon}}\,\tau(\hat{k},\hat{\epsilon})\frac{d^2\sigma^{\Gamma_0}}{d\Omega_{\hat{k}}d\Omega_{\hat{\epsilon}}}}{\int d\Omega_{\hat{k}}\int d\Omega_{\hat{\epsilon}}\frac{d^2\sigma^{\Gamma_0}}{d\Omega_{\hat{k}}d\Omega_{\hat{\epsilon}}}}. \tag{12}$$

III. PHOTODETACHMENT OF CORE ELECTRONS IN C_2^-

Narrow shape resonances at energies close to threshold are rare in photoionization, but are often found when the ejected electron leaves a neutral target behind. C_2^- offers an interesting test case in the present context, since both previous experiment and theory [50] have confirmed the presence of overlapping shape resonances in the total photodetachment cross section with $\approx$ 1-eV widths within 2 eV of threshold. Since the complex Kohn calculations on which the present results are based were described in some detail in Ref. [50], we will limit ourselves here to a brief summary. The ground-state anion is nominally described by the configuration $1\sigma_g^2 1\sigma_u^2 2\sigma_g^2 2\sigma_u^2 1\pi_u^4 3\sigma_g$, $^2\Sigma_g^+$. The neutral core-hole states arising from the $1\sigma_g$ and $1\sigma_u$ orbitals, being nearly degenerate, were both included in the close-coupling expansion. The singly occupied $1\sigma_g$ and $1\sigma_u$ orbitals can be either singlet

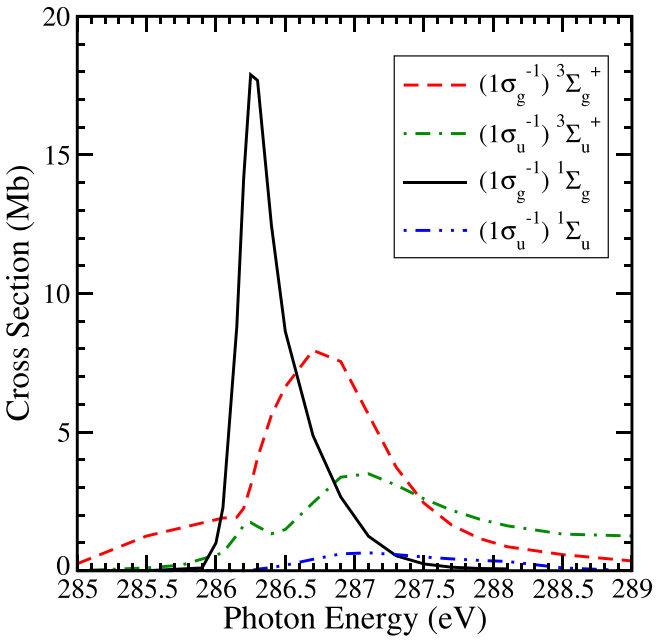

(a)

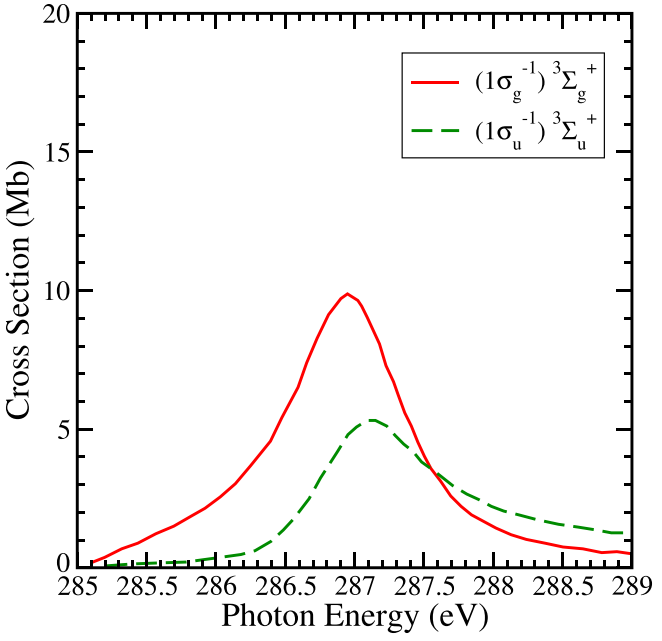

(b)

FIG. 2. Total cross sections for photodetachment of C_2^-. The calculations were performed in total $^2\Pi_u$ symmetry and the channels are labeled by neutral core-hole state. The top panel shows the results of coupled four-channel calculations, while the lower panel shows the result when channels 3 and 4 are dropped from the calculations (see text).

or triplet coupled to the outer valence $3\sigma_g$ orbital, giving neutral core-hole states of $^{1,3}\Sigma_g^+$ and $^{1,3}\Sigma_u^+$ symmetry.

The molecular orbitals used in the calculations were obtained in several steps as follows. We started with a complete active space (CAS) multiconfiguration self-consistent field (MCSCF) calculation on the $^2\Sigma_g^+$ state of C_2^-, freezing the $1\sigma_g$ and $1\sigma_u$ orbitals and using eight orbitals in the active space. This calculation was followed by a single multireference configuration-interaction (MRCI) calculation to obtain the four lowest-energy hole states. The MRCI calculation used the four neutral hole-state configurations mentioned above as the reference configurations and included single excitations from these references with the restriction that there be no more than three electrons distributed over the $1\sigma_g$ and $1\sigma_u$ orbitals. State-averaged natural orbitals were extracted from the MRCI calculation and were used to construct single-configuration approximations to the neutral hole states for the scattering calculation.

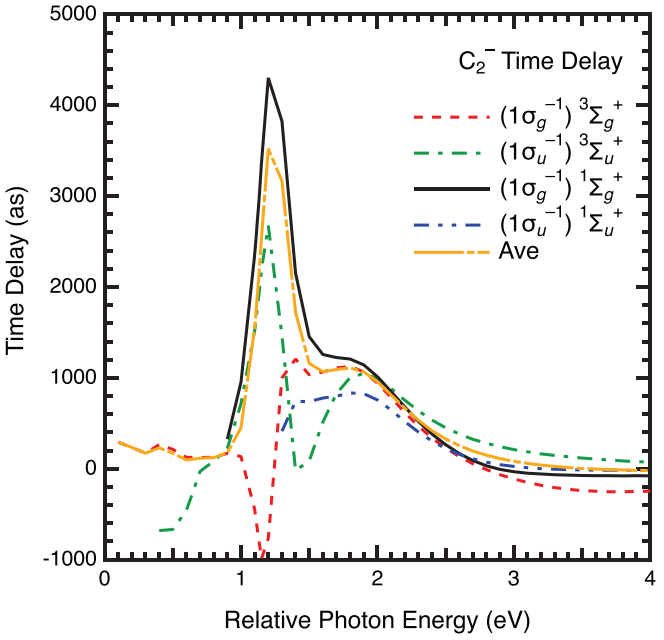

FIG. 3. C_2^- orientation-averaged time delays from four-channel calculations described in text. Photon energy is relative to 285 eV. The curve labeled "Ave" is the average of the four individual channel delays, weighted by the cross sections, as would be observed in an experiment not resolving the channels.

Total photodetachment cross sections, labeled by residual neutral core-hole state, are shown in Fig. 2. The cross sections are seen to be dominated by a narrow shape resonance in the $^1\Sigma_g^+$ channel and broader resonances in the $^3\Sigma_g^+$ and $^3\Sigma_u^+$ channels. The curious behavior in the latter two channel cross sections near 286.2-eV photon energy is caused by strong coupling to the $^1\Sigma_g^+$ channel, which results in a dip in the $^3\Sigma_g^+$ cross section and a shoulder in the $^3\Sigma_u^+$ cross section. To verify the cause of this effect, we carried out two-coupled-channel calculations in which the upper two core-ion states were eliminated. The lower panel of Fig. 2 verifies that so doing removes the structure near 286.2 eV.

The time delays, derived from the four-channel calculations and averaged over all molecular orientations, are shown in Fig. 3, labeled again by residual neutral core-hole state. The low-energy shape resonances in the partial cross sections in Fig. 2 are clearly visible in the large low-energy time delays, as are the consequences in the time delays of the strong channel coupling, described above. The large negative time delay in the $^3\Sigma_g^+$ channel, for example, is associated with that coupling and the accompanying interference with background scattering in that channel.

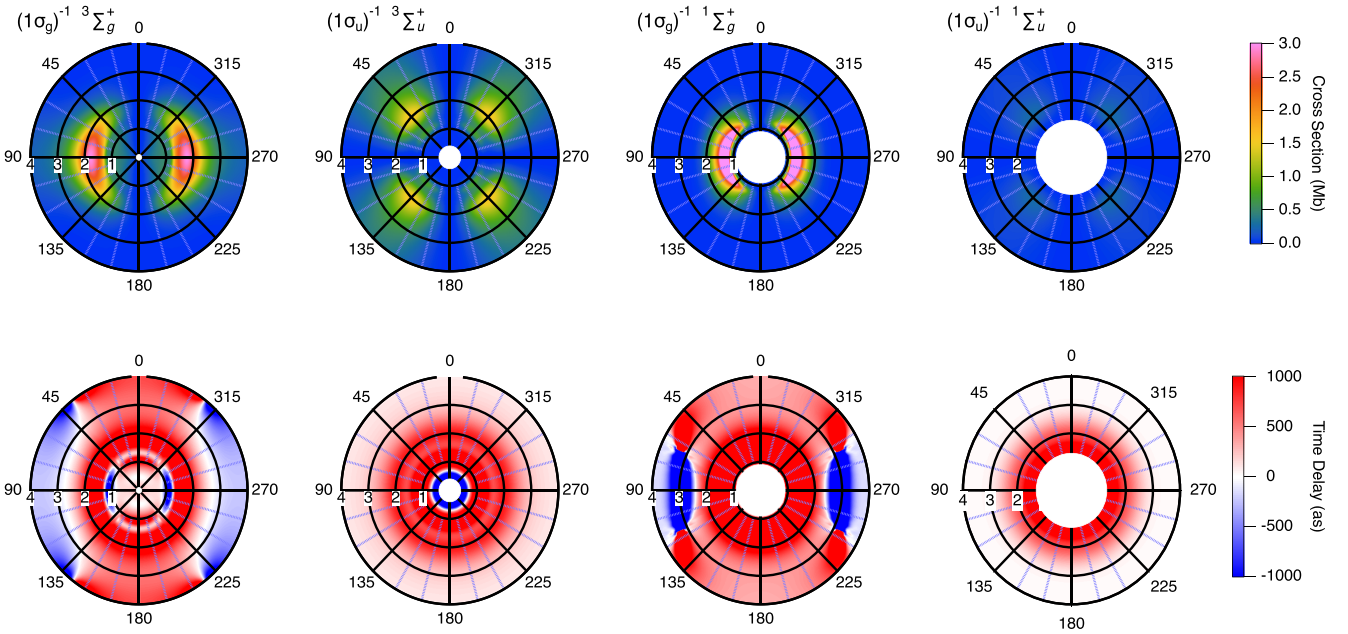

FIG. 4. MFPADs (top row) and time delays (bottom row) for photodetachment of C_2^- in each of the four channels included in the calculations in Figs. 2 and 3. From left to right results are given for leaving the molecule in the $^3\Sigma_g^+$, $^3\Sigma_u^+$, $^1\Sigma_g^+$, and $^1\Sigma_u^+$ states. The molecule is vertical, the polarization is horizontal, and photon energies labeled in eV by integers in the radial direction are relative to 285 eV, as are the energies given in Fig. 3.

Finally, in Fig. 4, we show cross sections and time delays, differential in energy and photoelectron direction, for photon polarization perpendicular to the C-C axis. One expects that the time delays associated with resonances will show little dependence on the direction of the ejected electron if the resonance dominates and there is little interference between resonant and background scattering. That is largely what is seen for the three higher-energy channels, but notably not for the $^3\Sigma_g^+$ channel, for which the signature of interference between resonant and nonresonant scattering is again apparent.

IV. PHOTODETACHMENT OF CORE ELECTRONS IN CN^-

Core-level photodetachment of CN^- offers an interesting test case for study as it differs from C_2^- in several key re-

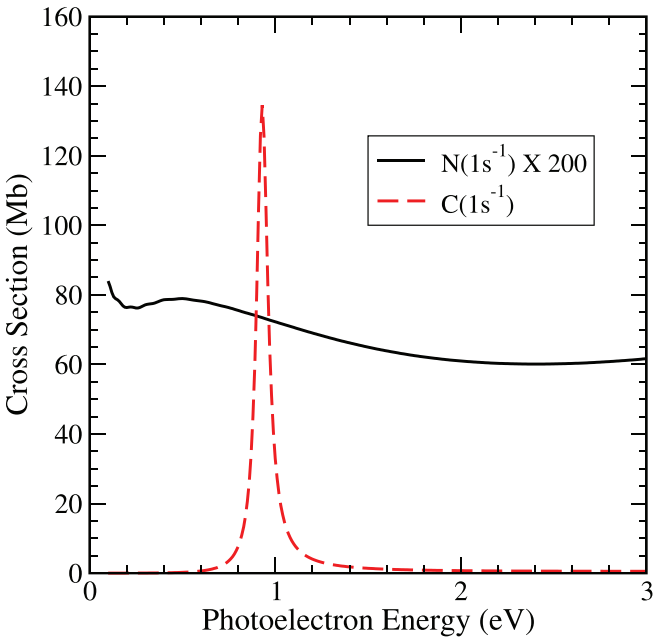

FIG. 5. Total cross sections for $C(1s^{-1})$ and $N(1s^{-1})$ photodetachment of CN^-.

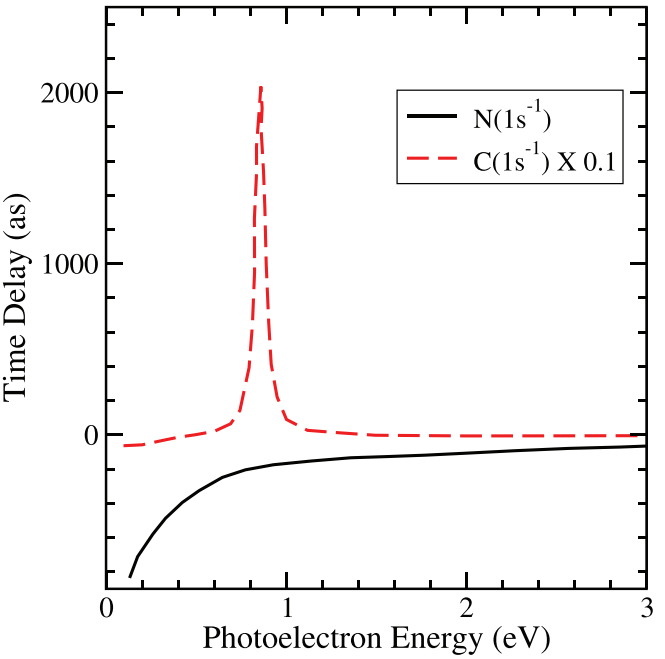

FIG. 6. Orientation-averaged time delays for $C(1s^{-1})$ and $N(1s^{-1})$ photodetachment of CN^-.

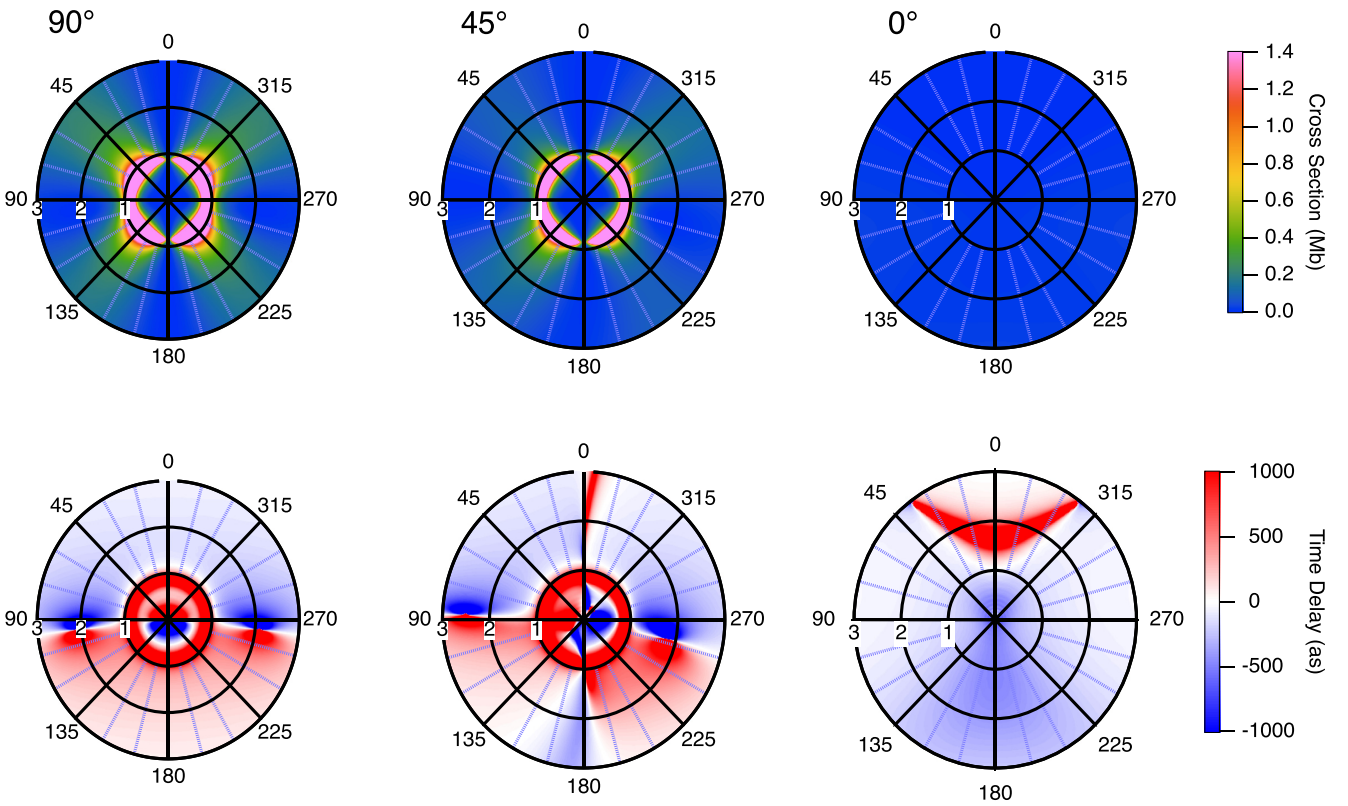

FIG. 7. MFPADs (top row) and time delays (bottom row) for CN^- for C K-edge photodetachment with two frozen MCSCF orbitals. The photoelectron energy in eV is labeled in the radial direction. The molecule is aligned vertically with nitrogen at the top, and polarization is at (left to right) 90°, 85°, 45°, and 0°.

spects. CN^- is a closed-shell anion with $^1\Sigma^+$ symmetry, so unlike the case with C_2^- only one intermediate spin coupling (i.e., $^2\Sigma^+$) is involved in C($1s$) or N($1s$) detachment. Another key difference is the fact that the residual CN neutral produced in photodetachment has a dipole moment whose sign depends on whether an electron is removed from either carbon or nitrogen. One might expect a signature at low energies of the interaction of the outgoing electron with those dipoles, although that is only one contribution to the asymmetry of the interaction potential. The present theoretical paper is meant to stimulate further study of the question of the roles of long- and short-range forces in determining photodetachment time delays.

The molecular orbitals used in these calculations were generated as follows. We started with a CAS-MCSCF calculation on neutral CN with seven strongly occupied orbitals plus three orbitals in the active space. The Gaussian basis used consisted of triple-zeta correlation-consistent plus polarization functions on C and N (f functions deleted), augmented with three additional s-type and three additional p-type diffuse functions at the bond center. The MCSCF orbitals were used to compute a single-configuration CN^- target state and in the complex Kohn scattering calculations by placing a single electron in either the C or N core.

The total cross sections for C($1s^{-1}$) and N($1s^{-1}$) are shown in Fig. 5 as a function of photoelectron energy and the orientation-averaged time delays are shown in Fig. 6. The carbon K-edge cross sections show a prominent π^* resonance approximately 1 eV above the K edge, which is reflected in a correspondingly large, positive time delay. There is little structure in the nitrogen K-edge results. The $1s \rightarrow \pi^*$ state which appears as a narrow shape resonance in the case of carbon falls ≈3 eV below the K edge in the case of nitrogen, resulting in no more than a small rise in the cross section and a negative time delay as the K edge is approached.

A deeper understanding of these results is gained from an examination of the cross sections and time delays in the body frame as a function of photoelectron energy and ejection angle for various angles of photon polarization. Turning first to the C K-edge results, shown in Fig. 7, we see a cross section dominated by a π^* resonance with predominantly d-wave character whose magnitude decreases as the photon polarization decreases from 90° and vanishes at 0°. The time delays show a similar decrease in magnitude as a function of photon polarization, with additional detail not apparent in the cross section. There is a curious reversal in the sign of the time delay along the molecular axis, most prominent at 90° photon polarization, as the electron energy sweeps through the resonance region. The behavior of the N K-edge cross sections and time delays, shown in Fig. 8, differs markedly from the C K-edge results. The lack of a resonance in the N K-edge case leads to asymmetric cross sections with small magnitudes on the carbon side of the molecule. This pattern differs from the C K-edge case which shows cross sections equally distributed

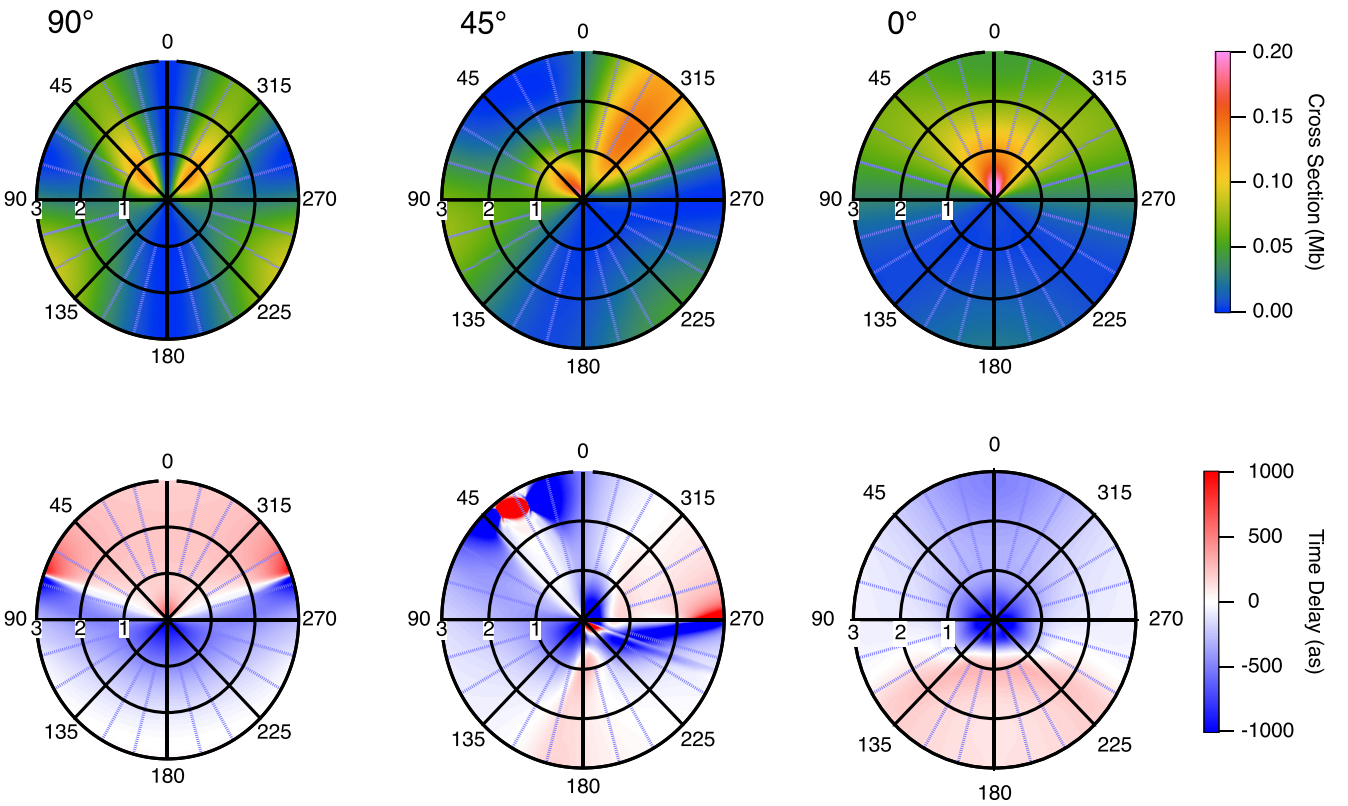

FIG. 8. MFPADs (top row) and time delays (bottom row) for CN^- for N K-edge photodetachment with two frozen MCSCF orbitals. The photoelectron energy in eV is labeled in the radial direction. The molecule is aligned vertically with nitrogen at the top, and polarization is at (left to right) 90°, 85°, 45°, and 0°.

over both sides of the molecule even though symmetry considerations do not dictate such behavior.

The "equivalent core" model for core ionization suggests a qualitative explanation that is consistent with this observation. Removal of a carbon 1s electron would be modeled in that approximation by changing the nuclear charge to that of nitrogen, while retaining the number of electrons in CN^- prior to photodetachment. Applying that approximate picture here suggests that the potential seen by the outgoing electron is similar to that of an electron scattering from N_2, for which the two ends of the molecule are equivalent. On that basis, one then would expect the nearly symmetric MFPADs in Fig. 7. Removal of a nitrogen 1s electron in the same approximation would produce an asymmetric model interaction potential similar to that of CO.

Comparing the time delays along the C-N axis in Figs. 7 and 8 we see, for perpendicular photon polarization, a sign change in the delay in the nitrogen K-edge case, while away from resonance the carbon K-edge delays show a similar behavior. However, in the case of the nitrogen K edge, the time delay changes from negative to positive in passing from carbon to nitrogen, while in the carbon K-edge case away from resonance the sign change passes from positive to negative. These calculations suggest initially that this behavior could be a reflection of the different dipole moments of the CN radical with core vacancies, because we compute a dipole moment of -0.92 (a.u.) for CN with a carbon core hole and a dipole moment of 1.28 (a.u.) for CN when the core hole is on the nitrogen.

V. INTERPRETATION OF PHOTODETACHMENT TIME DELAYS

It is tempting to interpret the low-energy time delays in photodetachment in terms of the long-range interaction of the electron with the molecule, in particular the reversal of the delays for CN^- detachment seen in the lower left-hand panels of Figs. 7 and 8. However, it is not difficult to demonstrate that such a simple interpretation of photodetachment time delays for photoelectron energies of a few eV is almost certainly not correct. An analysis of photodetachment delays requires an understanding of how the initial state in the dipole matrix element in Eq. (1) also determines the delay. Merely changing the initial state can also reverse the delays, and we can verify that fact with a simple model of photodetachment into a pure dipole potential.

The quantum scattering of an electron from a point-dipole potential $V_d = -d\cos\theta/r^2$ is well understood [51–55]. A natural model to test whether photodetachment time delays like those in Figs. 7 and 8 have simple interpretations in terms of the delay due to the long-range dipole interaction is to evaluate the delays from the dipole matrix element in Eq. (1) for various initial states but with the same continuum wave function for dipole scattering. Examining delays for different initial states then exhibits the effect of different ways of launching the photoelectron into the same continuum.

The dipole moments for our two core-detached neutral states of CN^- both have computed dipole moments that are greater than the critical value of $\approx 0.639 e\, a_0 = 1.62$ D. For

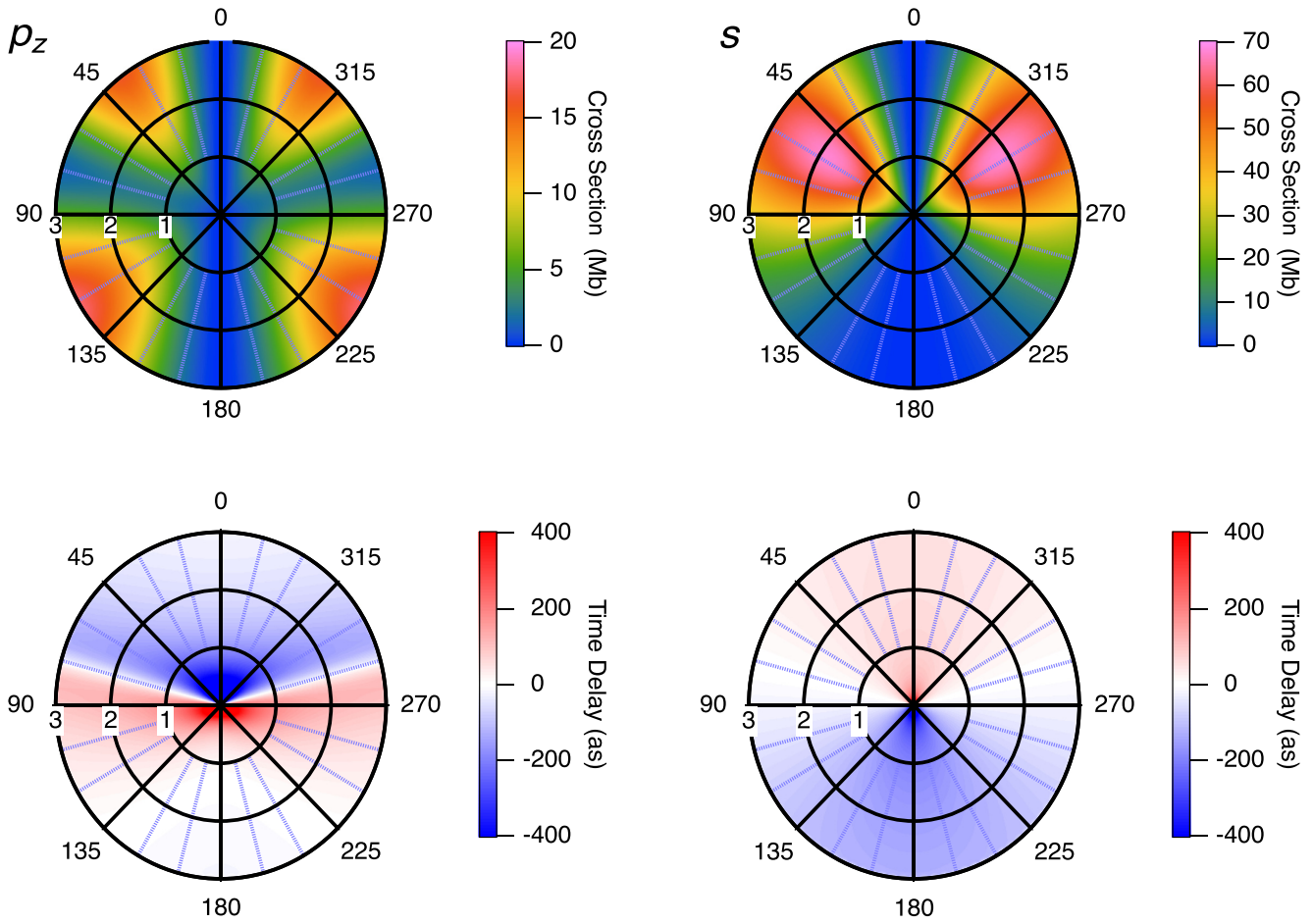

FIG. 9. Time delays and MFPADs for photodetachment in the model problem described by Eqs. (13) and (14) with only a dipole potential determining the final continuum and polarization perpendicular to the axis of the dipole. Left column: p_z initial state. Right column: s initial state with the same dipole potential.

dipole moments greater than that critical value the scattering solutions for a point dipole become irregular [51,52,54] as $r \to 0$, and the S matrix for scattering by a point dipole becomes nonunitary (see the Appendix). For that reason, and so that we can demonstrate delays for dipole moments approximating those of our computational examples, in a simple model we use a dipole potential regularized at small values of r according to

$$V = \begin{cases} -\frac{d\,\cos\theta}{r^2} & r \geqslant r_0 \\ -\frac{d\,\cos\theta}{r_0^2} & r < r_0 \end{cases} \tag{13}$$

so that the dipole points along the z axis with the parameters $r_0 = 0.25$ and $d = 1.5$ in atomic units. We choose two initial-state wave functions:

$$\Psi_0(\mathbf{r}) = \sqrt{\frac{8}{45}} r^2 e^{-r}\, Y_{\ell,m}(\theta,\phi), \tag{14}$$

with an s function ($\ell = m = 0$) and a p_z function pointing along to the dipole ($\ell = 1, m = 0$). The photodetachment amplitude can be extracted from a numerical solution of the driven equation for the first-order wave function, $\Psi_{\rm sc}(\mathbf{r})$:

$$(E_k - H)\Psi_{\rm sc}(\mathbf{r}) = \hat{\epsilon}\cdot\boldsymbol{\mu}\,\Psi_0(\mathbf{r}),$$

$$\Psi_{\rm sc}(\mathbf{r}) \underset{r\to\infty}{\longrightarrow} -\sqrt{2\pi}\frac{e^{ikr}}{r}\langle\Psi_{\mathbf{k}}^{-}|\hat{\epsilon}\cdot\boldsymbol{\mu}\,|\Phi_0\rangle, \quad \mathbf{k} = k\hat{\mathbf{r}}, \tag{15}$$

which we solve using the well-established finite-element discrete variable representation with exterior complex scaling and a single center expansion of the scattered wave function, as explained in detail in earlier literature [56,57].

So as to coincide with the geometry of polarization and dipole moment in the leftmost panels of Figs. 7 and 8 we choose the polarization along the y axes, perpendicular to the "molecule." Figure 9 compares the time delays and MFPADs for the s and p_z initial states in Eq. (14). It is evident that changing only the initial state produces a reversal in the time delays similar to that seen in Figs. 7 and 8.

It is apparent from computational experiments using model potentials such as this one that photodetachment time delays cannot be interpreted in terms of the final-state interactions alone. Moreover, for the wavelengths of electrons corresponding to kinetic energies of a few eV the interpretation of either

photodetachment delays or Wigner scattering delays in terms of locally attractive or repulsive potentials corresponds to a semiclassical approximation of the scattering dynamics that is simply not generally applicable at these energies. The dipole potential in particular resists this sort of analysis of its time delays, because, as we show briefly in the Appendix, the Wigner time delay is zero for scattering from a (subcritical) point dipole, but not for a combination of a point dipole and a short-range potential, and not for photodetachment into the point-dipole continuum.

To our knowledge, no successful simple prescription has been proposed for describing attosecond time delays in either photodetachment or photoionization that would allow the interpretation of such experiments without the help of *ab initio* theoretical calculations. Nonetheless, experiments measuring photoionization time delays have been performed comparing cases in which primarily the initial states are different while the final states may be similar, for example in water clusters [23], and those delays appear to be approximately interpretable in terms of the differences in the initial states alone. Even without simple semiclassical or other models, the potential of low-energy photodetachment experiments to probe with exquisite sensitivity electron-molecule interactions as well as the effects of correlation in the initial and continuum electronic states is evident in the examples we provide in Secs. IV and III.

VI. CONCLUSIONS

The electron scattering and photodetachment calculations presented here demonstrate that, in the absence of the dominating effects of the Coulomb potential in photoionization, a range of distinctly molecular features should be visible in photodetachment time delays. By focusing on photodetachment of electrons from core levels, we have provided examples where a subfemtosecond detaching pulse can produce photoelectrons with low energies where long-lived shape resonances abound in electron-molecule collisions. We predict in these calculations that low-energy photodetachment measurements can observe delays considerably longer than 1 fs and also measure dramatic asymmetries that reflect the combination of electron-molecule scattering and the initial orbital from which the electron is ejected. Such core-electron photodetachment experiments have the potential to initiate Auger decay and subsequent dissociation of a diatomic molecule into a neutral atom and an ion that can be observed in coincidence with the photoelectron, and, in principle, thus allow access to time delays in the molecular frame.

The measurement of delays in photodetachment of core electrons is arguably on the threshold of becoming practical, and the measurement using RABBITT of photodetachment delays has been analyzed in detail in the case of atomic anions [24] as briefly described in Sec. II A. At low photoelectron energies (below roughly 5 eV), measurements using that technique may require the prediction of the contribution to the observed delays from the associated continuum-continuum IR transition, but at higher energies those delays are expected to be negligible and photodetachment delays should be directly accessible.

The time delays in the molecular frame we report here are intended to raise the possibility of such experiments and suggest the effects they might reveal. We are currently exploring time delays in valence photodetachment from small polyatomic anions, where similarly dramatic molecular effects can be seen. Observations of photodetachment time delays for small polyatomic molecules will test *ab initio* theoretical treatments electron-molecule scattering at a level of detail not previously attained, because they will probe both the amplitude and the energy dependence of the phases of scattering amplitudes that are sensitive measures of correlation effects in electronic collisions.

ACKNOWLEDGMENTS

T.N.R, R.R.L., and C.W.M. were supported by the Atomic, Molecular, and Optical Sciences Program of the U.S. Department of Energy (DOE), Office of Science, Office of Basic Energy Sciences, Chemical Sciences, Geosciences, and Biosciences Division, through Contract No. DE-AC02-05CH11231. Calculations presented here made use of the resources of the National Energy Research Scientific Computing Center, a DOE Office of Science User Facility, and the Lawrencium computational cluster resource provided by the IT Division at LBNL. C.S.T. was supported by the U.S. DOE, Office of Science, Office of Workforce Development for Teachers and Scientists (WDTS) under the Berkeley Lab Undergraduate Faculty Fellowship (BLUFF) program.

APPENDIX: DIPOLE SCATTERING AND TIME DELAYS

To calculate the S matrix for scattering from a point dipole, we begin with the Hamiltonian

$$H = -\frac{1}{2}\frac{1}{r^2}\frac{\partial}{\partial r}r^2\frac{\partial}{\partial r} + \frac{\hat{L}^2}{2r^2} - \frac{d\cos\theta}{r^2} \tag{A1}$$

and expand the scattering wave function in partial waves,

$$\Psi^{(+)}(\mathbf{k},\mathbf{r}) = \left(\frac{2}{\pi}\right)^{1/2}\sum_{l,l_0,m_0} i^{l_0}\frac{\varphi^{m_0}_{l,l_0}(k,r)}{kr}Y_{lm_0}(\hat{\mathbf{r}})Y^*_{l_0m_0}(\hat{\mathbf{k}}), \tag{A2}$$

noting that the dipole potential does not couple different values of m_0. Substitution of Eq. (A2) into the Schrödinger equation with the Hamiltonian in Eq. (A1) yields sets of coupled equations for the radial functions $\varphi^{m_0}_{l,l_0}(k,r)$ for each value of m_0:

$$\begin{aligned}
&\sum_l\left[-\frac{1}{2}\frac{\partial^2}{\partial r^2}\delta_{l',l} + \frac{1}{r^2}V^{|m_0|}_{l',l}\right]\varphi^{|m_0|}_{l,l_0}(k,r) = E\varphi^{|m_0|}_{l',l_0}(k,r),\\
&V^{|m_0|}_{l',l} = \delta_{l',l}\frac{l(l+1)}{2} + d^{|m_0|}_{l'l},\\
&d^{|m_0|}_{l'l} \equiv -d\left\langle Y_{l'm_0}\right|\cos\theta\left|Y_{lm_0}\right\rangle.
\end{aligned} \tag{A3}$$

From this point, the solution of the scattering problem proceeds as follows. First, we find the eigenvectors and eigen-

values of the tridiagonal coupling matrix $V_{l',l}^{|m_0|}$:

$$\sum_l V_{l',l} U_{l,L} = U_{l',L} \Lambda_L,$$
$$\frac{L(L+1)}{2} = \Lambda_L, \quad L = -\frac{1}{2} + \left(\frac{1}{4} + 2\Lambda_L\right)^{1/2}, \tag{A4}$$
$$\mathbf{VU} = \mathbf{U\Lambda},$$
$$\mathbf{U}^T\mathbf{U} = \mathbf{UU}^T = \mathbf{1}.$$

So when we transform the radial equations in Eq. (A3) using the matrix $\mathbf{U}$, each eigenvalue, Λ_L, of $\mathbf{V}$ corresponds to a noninteger effective angular momentum, L, for one of the uncoupled transformed radial equations. The regular solutions for each equation in the diagonal representation are

$$\bar{\varphi}_L(k, r) = \hat{h}_L^-(kr) - \hat{h}_L^+(kr) = -2i\hat{j}_L(kr) \tag{A5}$$

where $\hat{h}_L^\pm$ and $\hat{j}_L$ denote Ricatti Bessel functions (see, e.g., Ref. [58]). We need to transform these back to the original representation, *and* find the linear combinations of the resulting back-transformed solutions that satisfy scattering boundary conditions [58]:

$$\varphi_{l,l_0}^{|m_0|}(k, r) = \hat{h}_l^-(kr)\,\delta_{l,l_0} - S_{l,l_0}^{|m_0|}\hat{h}_l^+(kr). \tag{A6}$$

The final result for the S matrix for each value of m_0, $\mathbf{S} = S_{l,l_0}^{|m_0|}$, when we include N partial waves is

$$\mathbf{S} = \mathbf{PUL}^{-2}\mathbf{U}^T\mathbf{P}, \tag{A7}$$

and the physical scattering solutions, arranged as columns of the matrix $\boldsymbol{\varphi}^{\text{phys}}$, are

$$\begin{aligned}\boldsymbol{\varphi}^{\text{phys}} &= \left(\varphi_l^{l_{0,1}}, \varphi_l^{l_{0,2}}, \cdots \varphi_l^{l_{0,N}}\right) \\ &= \mathbf{U}(\mathbf{H}^- - \mathbf{H}^+)\mathbf{L}^{-1}\mathbf{U}^T\mathbf{P}, \\ \varphi_l^{l_0}(k, r) &\to \hat{h}_l^-(kr)\,\delta_{l,l_0} - S_{l,l_0}^{|m_0|}\hat{h}_l^+(kr).\end{aligned} \tag{A8}$$

We have written these solutions in terms of the diagonal matrices:

$$\mathbf{L} = \begin{pmatrix} e^{iL_1\pi/2} & 0 & 0 & \cdots \\ 0 & e^{iL_2\pi/2} & 0 & \cdots \\ 0 & 0 & \ddots & \cdots \\ \vdots & \vdots & & e^{iL_N\pi/2} \end{pmatrix}, \tag{A9}$$

$$\mathbf{P} = \begin{pmatrix} e^{il_1\pi/2} & 0 & 0 & \cdots \\ 0 & e^{il_2\pi/2} & 0 & \cdots \\ 0 & 0 & \ddots & \cdots \\ \vdots & \vdots & & e^{il_N\pi/2} \end{pmatrix}, \tag{A10}$$

$$\mathbf{H}^\pm = \begin{pmatrix} h_{L_1}^\pm(kr) & 0 & 0 & \cdots \\ 0 & h_{L_2}^\pm(kr) & 0 & \cdots \\ 0 & 0 & \ddots & \cdots \\ \vdots & \vdots & & h_{L_N}^\pm(kr) \end{pmatrix}. \tag{A11}$$

A key point is that since the transformation to the uncoupled radial equations does not depend on energy, none of the matrix factors of the S matrix in Eq. (A7) has any energy dependence, and thus $\mathbf{S}$ has no energy-dependent phase. *Therefore there is no Wigner time delay, as conventionally defined, for electron scattering from a subcritical, fixed-point dipole.* It should be remembered that the dipole potential is a long-range potential in the same sense as the Coulomb potential, and is accompanied by similar formal difficulties. Nonetheless, the demonstration in Ref. [2] that even for a Coulomb potential the time delay defined by Eq. (1) is observable suggests that this result has physical significance.

However, a dipole matrix element between any physically realizable initial state and the point-dipole continuum function, Eq. (A2), does have an energy-dependent phase. So while there is no conventionally defined Wigner time delay, there *is* a photodetachment time delay into the point-dipole continuum [59]. That time delay is essentially what is visible in the model calculations in Fig. 9, determined by the dipole interaction, but revealed by the projection onto the initial bound state.

The expression for the S matrix in Eq. (A7) can be used to exactly reproduce the momentum transfer cross sections calculated by Mittleman and von Holdt [51] below the critical dipole. As the dipole moment increases towards the critical value of $d \approx 0.639e\,a_0$, one or more of the eigenvalues of the coupling matrix becomes negative and, as is well known, beyond the critical dipole at least one of the values of L becomes complex. Defined by the scattering asymptotic form in Eq. (A8), the S matrix ceases to be unitary [51–55] and the scattering solution is no longer a regular solution since $\hat{j}_L(z)$ is irregular (infinitely oscillatory as $z \to 0$) for complex values of L. Those are the mathematical pathologies associated with a "collapse to the center" [51,54].

When we apply the same prescription for solving the problem for scattering of a point dipole plus a spherical hard sphere potential, we first find a hard-sphere S matrix given by

$$\mathbf{S}^0 = \begin{pmatrix} h_{L_1}^-(k\,r_0)/h_{L_1}^+(k\,r_0) & 0 & 0 \\ 0 & h_{L_1}^-(k\,r_0)/h_{L_1}^+(k\,r_0) & \vdots \\ \vdots & \cdots & \ddots \end{pmatrix}, \tag{A12}$$

and finally a complete scattering S matrix analogous to that in Eq. (A7):

$$\mathbf{S} = \mathbf{PUL}^{-1}\mathbf{S}^0\mathbf{L}^{-1}\mathbf{U}^T\mathbf{P}. \tag{A13}$$

For this problem, as for any problem in which a short-range potential is added to the point dipole, there is a nonzero Wigner scattering time delay. Here $\mathbf{S}^0$ given in Eq. (A12) is obviously energy dependent, and its energy-dependent phases are modified by the dipole interaction.

[1] See for example the Special Issue on Molecular-frame photoelectron angular distributions, edited by R. R. Lucchese and A. Stolow, J. Phys. B: At. Mol. Opt. Phys. **45**, 190201 (2012), and references therein.

[2] R. Pazourek, S. Nagele, and J. Burgdörfer, Attosecond chronoscopy of photoemission, Rev. Mod. Phys. **87**, 765 (2015).

[3] S. Haessler, B. Fabre, J. Higuet, J. Caillat, T. Ruchon, P. Breger, B. Carré, E. Constant, A. Maquet, E. Mével, P. Salières, R. Taïeb, and Y. Mairesse, Phase-resolved attosecond near-threshold photoionization of molecular nitrogen, Phys. Rev. A **80**, 011404(R) (2009).

[4] M. Hentschel, R. Kienberger, C. Spielmann, G. A. Reider, N. Milosevic, T. Brabec, P. Corkum, U. Heinzmann, M. Drescher, and F. Krausz, Attosecond metrology, Nature (London) **414**, 509 (2001).

[5] M. Schultze *et al.*, Delay in photoemission, Science **328**, 1658 (2010).

[6] K. Klünder, J. M. Dahlström, M. Gisselbrecht, T. Fordell, M. Swoboda, D. Guénot, P. Johnsson, J. Caillat, J. Mauritsson, A. Maquet, R. Taïeb, and A. L'Huillier, Probing single-photon ionization on the attosecond time scale, Phys. Rev. Lett. **106**, 143002 (2011).

[7] L. Argenti, Á. Jiménez-Galán, J. Caillat, R. Taïeb, A. Maquet, and F. Martín, Control of photoemission delay in resonant two-photon transitions, Phys. Rev. A **95**, 043426 (2017).

[8] V. Gruson, L. Barreau, Á. Jiménez-Galán, F. Risoud, J. Caillat, A. Maquet, B. Carré, F. Lepetit, J.-F. Hergott, T. Ruchon, L. Argenti, R. Taïeb, F. Martín, and P. Salières, Attosecond dynamics through a fano resonance: Monitoring the birth of a photoelectron, Science **354**, 734 (2016).

[9] M. Kotur, D. Guénot, Á. Jiménez-Galán, D. Kroon, E. W. Larsen, M. Louisy, S. Bengtsson, M. Miranda, J. Mauritsson, C. L. Arnold, S. E. Canton, M. Gisselbrecht, T. Carette, J. M. Dahlström, E. Lindroth, A. Maquet, L. Argenti, F. Martín, and A. L'Huillier, Spectral phase measurement of a Fano resonance using tunable attosecond pulses, Nat. Commun. **7**, 10566 (2016).

[10] C. Cirelli *et al.*, Anisotropic photoemission time delays close to a Fano resonance, Nat. Commun. **9**, 955 (2018).

[11] S. Banerjee, P. C. Deshmukh, V. K. Dolmatov, S. T. Manson, and A. S. Kheifets, Strong dependence of photoionization time delay on energy and angle in the neighborhood of Fano resonances, Phys. Rev. A **99**, 013416 (2019).

[12] F. Holzmeier, J. Joseph, J. C. Houver, M. Lebech, D. Dowek, and R. R. Lucchese, Influence of shape resonances on the angular dependence of molecular photoionization delays, Nat. Commun. **12**, 7343 (2021).

[13] L. Gallmann, I. Jordan, H. J. Wörner, L. Castiglioni, M. Hengsberger, J. Osterwalder, C. A. Arrell, M. Chergui, E. Liberatore, U. Rothlisberger, and U. Keller, Photoemission and photoionization time delays and rates, Struct. Dyn. **4**, 061502 (2017).

[14] P. Hockett, E. Frumker, D. M. Villeneuve, and P. B. Corkum, Time delay in molecular photoionization, J. Phys. B **49**, 095602 (2016).

[15] D. Baykusheva and H. J. Wörner, Theory of attosecond delays in molecular photoionization, J. Chem. Phys. **146**, 124306 (2017).

[16] D. Busto, J. Vinbladh, S. Zhong, M. Isinger, S. Nandi, S. Maclot, P. Johnsson, M. Gisselbrecht, A. L'Huillier, E. Lindroth, and J. M. Dahlström, Fano's propensity rule in angle-resolved attosecond pump-probe photoionization, Phys. Rev. Lett. **123**, 133201 (2019).

[17] J. Joseph, F. Holzmeier, D. Bresteau, C. Spezzani, T. Ruchon, J. F. Hergott, O. Tcherbakoff, P. D'Oliveira, J. C. Houver, and D. Dowek, Angle-resolved studies of XUV-IR two-photon ionization in the RABBITT scheme, J. Phys. B **53**, 184007 (2020).

[18] A. Kamalov, A. L. Wang, P. H. Bucksbaum, D. J. Haxton, and J. P. Cryan, Electron correlation effects in attosecond photoionization of CO_2, Phys. Rev. A **102**, 023118 (2020).

[19] J. Fuchs, N. Douguet, S. Donsa, F. Martin, J. Burgdörfer, L. Argenti, L. Cattaneo, and U. Keller, Time delays from one-photon transitions in the continuum, Optica **7**, 154 (2020).

[20] D. You *et al.*, New method for measuring angle-resolved phases in photoemission, Phys. Rev. X **10**, 031070 (2020).

[21] S. Heuser, A. Jiménez Galán, C. Cirelli, C. Marante, M. Sabbar, R. Boge, M. Lucchini, L. Gallmann, I. Ivanov, A. S. Kheifets, J. M. Dahlström, E. Lindroth, L. Argenti, F. Martín, and U. Keller, Angular dependence of photoemission time delay in helium, Phys. Rev. A **94**, 063409 (2016).

[22] S. Heck, M. Han, D. Jelovina, J.-B. Ji, C. Perry, X. Gong, R. Lucchese, K. Ueda, and H. J. Wörner, Two-center interference in the photoionization delays of Kr_2, Phys. Rev. Lett. **129**, 133002 (2022).

[23] X. Gong, S. Heck, D. Jelovina, C. Perry, K. Zinchenko, R. Lucchese, and H. J. Wörner, Attosecond spectroscopy of size-resolved water clusters, Nature (London) **609**, 507 (2022).

[24] E. Lindroth and J. M. Dahlström, Attosecond delays in laser-assisted photodetachment from closed-shell negative ions, Phys. Rev. A **96**, 013420 (2017).

[25] P. M. Paul, E. S. Toma, P. Breger, G. Mullot, F. Auge, P. Balcou, H. G. Muller, and P. Agostini, Observation of a train of attosecond pulses from high harmonic generation, Science **292**, 1689 (2001).

[26] S. Saha, J. Jose, P. C. Deshmukh, G. Aravind, V. K. Dolmatov, A. S. Kheifets, and S. T. Manson, Wigner time delay in photodetachment, Phys. Rev. A **99**, 043407 (2019).

[27] S. Saha, P. C. Deshmukh, A. S. Kheifets, and S. T. Manson, Dominance of correlation and relativistic effects on photodetachment time delay well above threshold, Phys. Rev. A **99**, 063413 (2019).

[28] R. Dörner, V. Mergel, O. Jagutzki, L. Spielberger, J. Ullrich, R. Moshammer, and H. Schmidt-Böcking, Cold target recoil ion momentum spectroscopy: A momentum microscope to view atomic collision dynamics, Phys. Rep. **330**, 95 (2000).

[29] T. Jahnke, Th. Weber, T. Osipov, A. L. Landers, O. Jagutzki, L. P. H. Schmidt, C. L. Cock, M. H. Prior, H. Schmidt-Böcking, and R. Dörner, Multicoincidence studies of photo and auger electrons from fixed-in-space molecules using the COLTRIMS technique, J. Electron Spectrosc. Relat. Phenom. **141**, 229 (2004).

[30] J. Ullrich, R. Moshammer, A. Dorn, R. Dörner, L. P. H. Schmidt, and H. Schmidt-Böcking, Recoil-ion and electron momentum spectroscopy: Reaction-microscopes, Rep. Prog. Phys. **66**, 1463 (2003).

[31] L. Eisenbud, Formal properties of nuclear collisions, Ph.D. thesis, Princeton University, 1948.

[32] E. P. Wigner, Lower limit for the energy derivative of the scattering phase shift, Phys. Rev. **98**, 145 (1955).

[33] F. T. Smith, Lifetime matrix in collision theory, Phys. Rev. **118**, 349 (1960).

[34] C. de Carvalho and H. Nussenzveig, Time delay, Phys. Rep. **364**, 83 (2002).

[35] H. M. Nussenzveig, Time delay in quantum scattering, Phys. Rev. D **6**, 1534 (1972).

[36] The steps to derive Eq. (1) directly from the long-time limit of Eq. (5) require replacing $\psi^{-}_{\Gamma,\vec{k}_\Gamma}$ by its incoming wave scattering asymptotic form, then using the asymptotic form of the plane wave $\exp(i\vec{k}_\Gamma \cdot \vec{r}) \to \frac{2\pi}{ik_\Gamma r}(\delta(\hat{\mathbf{k}}_\Gamma - \hat{\mathbf{r}})e^{ik_\Gamma r} - \delta(\hat{\mathbf{k}}_\Gamma + \hat{\mathbf{r}})e^{-ik_\Gamma r}) + \mathcal{O}(1/r^2)$ as in Ref. [35], and finally expanding the phase of the matrix element $D_\Gamma(\vec{k}_\Gamma)$ linearly around the central energy of the laser pulse.

[37] T. Seideman, Rotational excitation and molecular alignment in intense laser fields, J. Chem. Phys. **103**, 7887 (1995).

[38] H. Stapelfeldt and T. Seideman, *Colloquium:* Aligning molecules with strong laser pulses, Rev. Mod. Phys. **75**, 543 (2003).

[39] Y. Ohshima and H. Hasegawa, Coherent rotational excitation by intense nonresonant laser fields, Int. Rev. Phys. Chem. **29**, 619 (2010).

[40] T. Driver *et al.*, Attosecond delays in x-ray molecular ionization (unpublished).

[41] R. N. Zare, Photoejection dynamics, Mol. Photochem. **4**, 1 (1972).

[42] R. N. Zare, Dissociation of H_2^+ by electron impact: Calculated angular distribution, J. Chem. Phys. **47**, 204 (1967).

[43] S. Nagele, R. Pazourek, J. Feist, K. Doblhoff-Dier, C. Lemell, K. Tőkési, and J. Burgdörfer, Time-resolved photoemission by attosecond streaking: Extraction of time information, J. Phys. B **44**, 081001 (2011).

[44] J. Dahlström, D. Guénot, K. Klünder, M. Gisselbrecht, J. Mauritsson, A. L'Huillier, A. Maquet, and R. Taïeb, Theory of attosecond delays in laser-assisted photoionization, Chem. Phys. **414**, 53 (2013).

[45] T. N. Rescigno, B. H. Lengsfield, and C. W. McCurdy, in *Modern Electronic Structure Theory*, edited by D. R. Yarkony (World Scientific, Singapore, 1995), Vol. 1, pp. 501–588.

[46] T. N. Rescigno, B. H. Lengsfield, and A. E. Orel, Interchannel coupling and ground state correlation effects in the photoionization of CO, J. Chem. Phys. **99**, 5097 (1993).

[47] S. Miyabe, C. W. McCurdy, A. E. Orel, and T. N. Rescigno, Theoretical study of asymmetric molecular-frame photoelectron angular distributions for C1s photoejection from CO_2, Phys. Rev. A **79**, 053401 (2009).

[48] T. N. Rescigno, N. Douguet, and A. E. Orel, Imaging molecular isomerization using molecular-frame photoelectron angular distributions, J. Phys. B **45**, 194001 (2012).

[49] C. S. Trevisan, C. W. McCurdy, and T. N. Rescigno, Imaging molecular geometries with molecular frame photoelectron angular distributions from core hole ionization, J. Phys. B **45**, 194002 (2012).

[50] N. Douguet, S. Fonseca dos Santos, and T. N. Rescigno, Inner-shell photodetachment of C_n^- ions, Phys. Rev. A **101**, 033411 (2020).

[51] M. H. Mittleman and R. E. von Holdt, Theory of low-energy-electron scattering by polar molecules, Phys. Rev. **140**, A726 (1965).

[52] J.-M. Lévy-Leblond, Electron capture by polar molecules, Phys. Rev. **153**, 1 (1967).

[53] W. R. Garrett, Scattering by a dipolar system: Divergence of cross sections at the critical moment for a point dipole rotor, Phys. Rev. A **23**, 1737 (1981).

[54] T. Wasak and Z. Idziaszek, Quantum reactive scattering in the long-range ion-dipole potential, Phys. Rev. A **103**, 023324 (2021).

[55] A. Herzenberg, Singularities in the scattering of a very slow electron by a weakly polar molecule, J. Phys. B **17**, 4213 (1984).

[56] T. N. Rescigno and C. W. McCurdy, Numerical grid methods for quantum-mechanical scattering problems, Phys. Rev. A **62**, 032706 (2000).

[57] C. W. McCurdy, M. Baertschy, and T. N. Rescigno, Solving the three-body Coulomb breakup problem using exterior complex scaling, J. Phys. B **37**, R137 (2004).

[58] J. Taylor, *Scattering Theory: The Quantum Theory of Nonrelativistic Collisions*, Dover Books on Engineering (Dover, New York, 2006).

[59] Note that while the Wigner and photodetachment delays are related by a factor of 2 in the special case in which a single partial wave contributes to the photodetachment amplitude, that relation does not hold here because the dipole potential couples all partial waves with different l quantum numbers for the same m angular momentum quantum number. The scattering phase shift does not appear as an overall factor determining the phase of the dipole transition amplitude when more than one partial wave contributes.